*Journal of Applied Fluid Mechanics*, Vol. 12, No. 3, pp. 947-959, 2019.
Available online at www.jafmonline.net, ISSN 1735-3645, EISSN 1735-3645.
DOI: 10.29252/jafm.12.03.29525

# A Computational Fluid Dynamics Investigation on the Drag Coefficient Measurement of an AUV in a Towing Tank

E. Javanmard[1†] and Sh. Mansoorzadeh[2]

[1] *Department of Mechanical Engineering, Isfahan University of Technology, Isfahan, Iran*
[2] *Subsea Science & Technology Center, Isfahan University of Technology, Isfahan, Iran*

†*Corresponding Author Email: e.javanmard@me.iut.ac.ir*

(Received August 11, 2018; accepted October 2, 2018)

## ABSTRACT

The accuracy of experimental procedure used to calculate the drag coefficient of an Autonomous underwater vehicle (AUV) in a towing tank is investigated using computational fluid dynamics. Effects of struts, used to connect the AUV model to towing carriage, on the hydrodynamics coefficient of the AUV at various relative submergence depths, at AUV speeds of 1.5 and 2.5 m/s are numerically simulated. Various numerical modeling are performed to investigate the effects of free surface with and without presence of struts on the drag coefficient of the AUV. Volume of fluid (VOF) model is used to solve the two phase flow RANS equations. The drag coefficients obtained from two phase flow simulations are compared with those obtained from single phase flow at corresponding velocities. The results obtained from experiments conducted in the towing tank of the Subsea Science and Technology centre, on a full-scale model of the AUV developed in this Centre, agreed well with those obtained by numerical simulations.

**Keywords**: Free surface; AUV; Computational fluid dynamics; VOF; Towing tank; Strut.

## NOMENCLATURE

| | |
|---|---|
| $C_d$ | drag force coefficient |
| $C_P$ | pressure coefficient |
| $C_{Strut}$ | chord length of the struts (NACA0012) |
| $D$ | hull diameter |
| $F_d$ | drag force |
| $F_{(AUV)}$ | net resistance force of AUV |
| $F_{(Struts)}$ | total axial force exerted on the struts |
| $F_{(AUV+Struts)}$ | force exerted on the AUV and the struts |
| $h$ | distance of the free surface from the AUV upper surface |
| $h^*$ | relative submergence depth |
| $L$ | hull length |
| $P$ | pressure |
| $P_{ref}$ | reference pressure |
| SIM-2 | simulation of AUV when it moves under free surface, without considering any struts |
| SIM-3 | simulation of struts when they move in the towing tank alone |
| SIM-4 | simulation of AUV when it moves in an infinite medium |
| $\overline{\acute{U}_i\acute{U}_j}$ | reynolds stress |
| $Re_l$ | reynolds based on length |
| $S$ | reference surface area |
| $S_{AUV}$ | reference surface area for AUV |
| $S_{Strut}$ | reference surface area for Strut |
| SIM-1 | simulation of AUV and its struts when they move in the towing tank |
| $V$ | total volume |
| $\mathbf{V}$ | velocity vector |
| $V_i$ | volume of phase *i* |
| $\bar{V}$ | reference velocity |
| $v$ | towing speed or AUV speed |
| $\alpha_i$ | volume fraction of phase *i* |
| $\rho$ | density |
| $\rho_i$ | density of phase *i* |
| $\rho_m$ | bulk density |
| $\mu_m$ | bulk viscosity |
| $\delta_l$ | boundary layer thickness |
| $\Delta y$ | first layer thickness |
| $\Delta y^+$ | dimensionless First layer thickness |

## 1. INTRODUCTION

Autonomous underwater vehicles (AUVs) play an important role in different application fields, such as underwater surveys, environment monitoring, oceanographic studies, military, homeland defense, etc. Extensive use of AUVs in various maritime fields, therefore, necessitates investigation of their hydrodynamics performance. The hydrodynamics performance of AUVs as well as their navigation and control requires a better understanding of various forces acting on these vehicles under various conditions. Since various forces acting on these vehicles are expressed in terms of hydrodynamics coefficients, a great deal of researches was conducted on the subject of calculation of hydrodynamic coefficients of these vehicles. A number of methods have been reported for calculating the hydrodynamics coefficients of underwater vehicles. They include computational fluid dynamics (Hopkin and Den Hertog, 1993; Nahon, 1993; Bellevre *et al.*, 2000; Wu *et al*., 2005; Tyagi and Sen, 2006; Philips *et al.*, 2007; Broglia *et al*., 2007; Barros *et al*., 2008; Jagadeesh and Murali, 2010; Zhang *et al.*, 2010; Malik *et al.*, 2013; Mansoorzadeh and Javanmard, 2014), experimental (Jagadeesh *et al*., 2009; Julca Avila *et al.*, 2012; Zhang and Zou, 2013; Javanmard, 2013; Krishnankutty, 2014) and analytical and semi-empirical (ASE) methods (Jones and Clarke 2002; Peterson 1980). Although experimental methods seem to be the most accurate, relative to the other methods, they are associated with many sources of errors and uncertainties. For example, experimental results obtained in a towing tank suffer from errors associated with test setup, scale effects, model fabrication inaccuracies, calibration errors, tank wall effects, etc. On the other hand, the results obtained from numerical simulations suffer from inaccuracies in physical models and numerical errors. Judging which method is more accurate is not very straightforward. However, using both methods together and comparing the results can lead to more elaborate results. In this paper a set of numerical simulations was carried out in order to model the experiments usually conducted in towing tanks to calculate the drag force and its pertinent hydrodynamics coefficients of a submersible vessel. The effect of the free water surface and struts used to connect the model to the towing carriage, on the obtaining results are investigated. Since AUVs are designed to move in deep water, (far from the free surface), to calculate their hydrodynamic coefficients experimentally in a towing tank, free surface effects should be eliminated. Therefore the AUV model should be towed in a depth at which free surface effect is negligible. A set of experiments at various depths and speeds should, therefore, be conducted, to find a minimum depth at which the surface effect on hydrodynamic coefficients is negligible. To calculate the drag coefficient of an AUV in a towing tank, experimentally, a scaled model of the AUV is towed at various constant speeds. The resistance force is then measured by a dynamometer (force meter) at each speed. The drag coefficient can be calculated as:

$$C_d = F_d / 0.5\rho v^2 S \quad (1)$$

Where $F_d$ is the drag resistance force measured by the dynamometer, $\rho$ is the density of the water, $v$ is the towing speed and $S$ is the reference surface area. To tow the AUV model by the towing carriage at various speeds, it is usual to use one or two struts, as shown in Fig. 1 or to use a sting mechanism as shown in Fig. 2. A sting is a long shaft attaching the downstream end of the model so that it does not much disturb the flow over the model. The rear end of a sting usually has a conical fairing blending into the model support structure. In both cases, presence of struts or sting can disturb the flow around and behind the AUV model. Presence of struts changes the stream lines of the surrounding fluid. Therefore, the drag force measured by the load cell is influenced by the disturbance caused by the struts or sting. Although the disturbance of a sting is expected to be much lower than struts, the effect of AUV propeller cannot be investigated, when sting is installed behind the AUV. There is no direct experimental method to measure the effect of struts on the measured drag force. In order to minimize the disturbance of struts, stream lined NACA shaped struts are mostly used to connect the AUV model to the carriage load cells. On the other hand , if an external load cell is used to measure the resistance force, as indicated in Fig. 1, the force indicated by the load cell includes both AUV and strut resistance force. Therefore to obtain the net AUV resistance forces, an additional experiment should be conducted to calculate the resistance force of the struts alone, at each speed. This force should be subtracted from the force measured in the first experiment to obtain the net resistance force of the AUV.

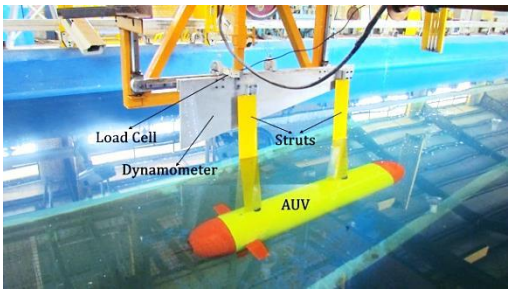


**Fig. 1. Experimental setup indicating AUV connected to the towing carriage using struts.**

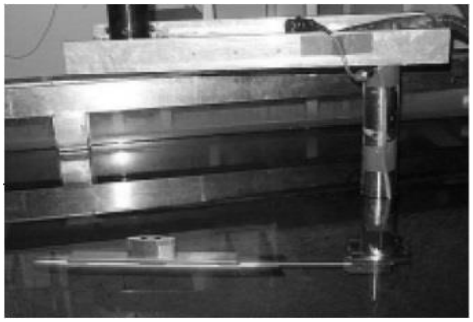

**Fig. 2. Application of sting mechanism in the towing tank tests (Rhee *et al*., 2000).**

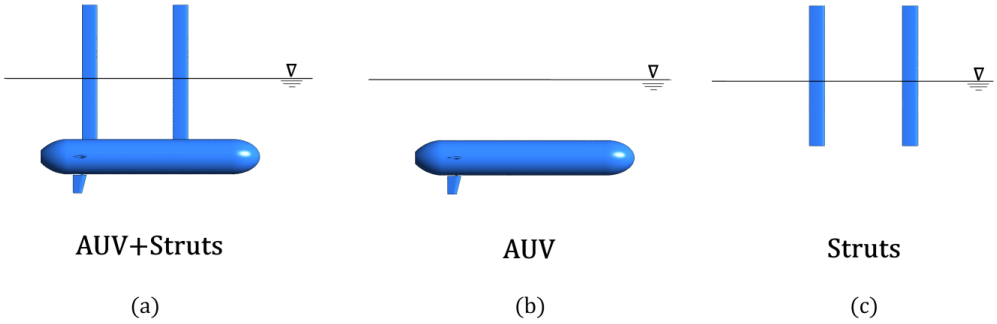


**Fig. 3. Various experimental configurations used to calculate the drag force of AUV, including: A schematic of an AUV model connected to the struts and towed with a constant speed, corresponding to numerical simulation SIM-1(a), A schematic of an AUV model without struts corresponding to numerical simulation SIM-2 (b), A schematic of struts towed with a constant speed, corresponding to numerical simulation SIM-3 (c).**

Now, the question is how accurate the results obtained by this experimental method are? Here we attempt to describe this problem in more details.

Figure 3(a) shows a schematic of an AUV model connected to the struts and towed with a constant speed. The resistance force that an external load cell measures is the total axial force exerted on the AUV and the struts. We indicate this force by $F_{(AUV+Struts)}$. Figure 3(c) shows a schematic of the struts towed with the same speed as in Fig. 3(a). The total axial force exerted on the struts can be measured by the load cell. We indicate this force by $F_{(Struts)}$. To obtain the net resistance force of the AUV alone, $F_{(AUV)}$, as shown in Fig. 3(b), the following assumption can be made:

$$F_{(AUV)} = F_{(AUV+Struts)} - F_{(Struts)} \tag{2}$$

Both $F_{(AUV+Struts)}$ and $F_{(Struts)}$ can be measured experimentally. However, $F_{(AUV)}$ can only be evaluated by Eq. (2). This force cannot be measured experimentally. For the following reasons $F_{(AUV)}$ obtained by Eq. (2) is only an approximation:

1. Presence of struts disturbs the stream lines around the AUV, therefore $F_{(AUV)}$ obtained by Eq. (2) is a result of disturbed stream line around the AUV.
2. Presence of AUV next to the struts disturbs the streamlines around struts, therefore, $F_{(Struts)}$ obtained from the experiment, conducted as shown in Fig. 3(c), differs from the force exerted on the struts connected to the AUV, as shown in Fig. 3(a).
3. Motion of AUV and struts near the free surface can create a wave on free surface. Wave making resistance, therefore, plays an important role on the total resistance force, sensed by the load cell. The motion resistance, in this case depends on the wave profile created on the free surface. The wave profile in Figs. 3(a), 3(b) and 3(c) might be different. Therefore each term in Eq. (2) is measured, or calculated, under different surface wave profile. This increases the uncertainties associated with Eq. (2).

In the present paper an attempt has been made to use CFD to justify the experimental procedure used for calculation of AUV drag. Computational fluid dynamics can be used to simulate the AUV motion in a towing tank and calculate the drag force of AUV and its struts, exactly in the same way it is measured experimentally, as shown in Fig. 3(a). We call this simulation SIM-1. It is also possible to use CFD to calculate the drag force of the AUV directly, when it moves under free surface, without considering any struts, as shown in Fig. 3(b). We call this simulation SIM-2. We can also numerically calculate the drag force of struts when they move in the towing tank, separately, in the same way that we measured it experimentally, as shown in Fig. 3(c). We call this simulation SIM-3. Comparing the results obtained for the drag forces of AUV and struts from numerical simulations SIM-2 and SIM-3, respectively, with corresponding values obtained from simulation SIM-1 shows how accurate Eq. (2) is for evaluation of the drag coefficient of the AUV. Another set of simulations, called SIM-4, is also performed, in which AUV moves in an infinite medium. There is no free surface effect in this case. The results obtained at various depths and speeds from simulations SIM-1 and SIM-2 can be compared with those of simulation SIM-4, to investigate the effect of free surface on the drag force. The accuracy of Eq. (2) is a function of shape of the AUV and its struts, its speed and the AUV distance from the free surface. This study was carried out for the AUV developed and constructed in the Subsea Research and Development center of Isfahan University of Technology (IUT), located in Iran. A photo of the AUV is shown in Fig. 4 and its main specifications are listed in Table 1. The simulations are performed for various submergence depth and two different speeds namely 1.5 m/s (nominal speed of the AUV) and 2.5 m/s, to investigate the effect of speed increase on the results. The two phase flow results are compared with the corresponding results obtained from the single phase flow simulations, performed for an infinite domain. The numerical results are then compared with the available experimental results conducted in the subsea R&D center of IUT.

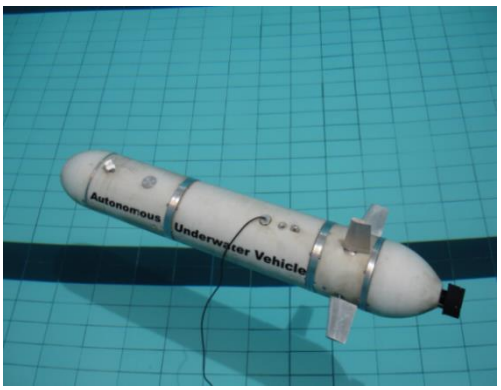


**Fig. 4. IUT Autonomous Underwater Vehicle.**

**Table 1 AUV Characteristics**

| Parameters | Description |
|---|---|
| Shape | Torpedo |
| Length(***L***) | 145 cm |
| Diameter(***D***) | 23 cm |
| Weight in air | 45 kg |
| Depth of operation | 200 cm |
| Time of operation | 2.5 hr |
| Fins shape | NACA0015 |
| Horizontal velocity | 3 knot |
| $S_{AUV}$ | 415.5 cm$^2$ |

## 2. EXPERIMENTAL SETUP

A fiber-glass full-scale model of the subsea R&D AUV was fabricated to conduct the experiments. The experiments were carried out in the IUT towing tank. The length, width and depth of the towing tank were 108, 3 and 2.2 m, respectively. The AUV model, as shown in Fig. 1, was connected to the carriage dynamometer through two Naca0012 struts with a chord length of $C_{Strut}$=10cm. The AUV model distance from the surface water could be adjusted by an elevator mechanism. Table 2 shows the various conditions in which experiments were carried out. In order to measure the net force exerted on the vessel body, experiments were carried out in two steps. In the first step, the force required to tow the AUV model together with its struts at a specified speed, was measured. In the second step, the forces required to tow only the struts, at the same speed, was measured. By subtracting the force measured in the second, from the one in the first step, the pure force required to tow only the vessel body was calculated.

## 3. NUMERICAL SIMULATIONS

### 3.1 Theoretical Background

To capture the free surface effects over the AUV numerically, the volume of fluid (VOF) method is adopted. The VOF method is one of the most popular schemes for tracking interfaces and locating the free surface (Lafaurie *et al*., 1994; Pilliod Jr and Puckett 1994; Rider and Kothe 1995, 1998; Scardovelli and Zaleski (1999). In this method, the data structure that represents the interface is the fraction $\alpha$ of each cell that is filled with a reference phase, say phase 1. The scalar field $\alpha$ is often referred to as the color function. We have $0 < \alpha < 1$ in cells cut by the interface and $\alpha = 0$ or 1 away from it. The data $\alpha$ are given at the beginning of a computational cycle but no approximation of the interface position is known (Gueyffier *et al*., 1999). To model the motion of the AUV under the water free surface, the equations governing the conservation of mass and moment of the air and water should be solved. With this background, the two phase flow conservation of mass and momentum equations can be expressed as Eq. (3) to Eq. (7) (ANSYS, 2009b).

$$\frac{\partial}{\partial t}(\alpha_i \rho_i) + \nabla.(\alpha_i \rho_i \mathbf{V}) = 0 \qquad i = 1,2 \tag{3}$$

$$\alpha_i = \frac{V_i}{V} \qquad i = 1,2 \tag{4}$$

$$\sum_i \alpha_i = 1.0 \tag{5}$$

$$\sum_i \nabla.(\alpha_i \mathbf{V}) = 0. \tag{6}$$

$$\frac{\partial}{\partial t}(\rho_m \mathbf{V}) + \nabla.(\rho_m \mathbf{V} \times \mathbf{V}) = \nabla.\left(-P + \mu_m \left((\nabla \mathbf{V}) + (\nabla \mathbf{V})^T\right)\right) \tag{7}$$

Where, $\alpha_i$, $\rho_i$ and $V_i$ are the volume fraction, density and volume of phase $i$, respectively. The velocity vector is denoted by $\mathbf{V}$, while, $V$ is the total volume. $\mu_m$ and $\rho_m$ are the bulk viscosity and density, respectively, and $P$ is the pressure. The volume fraction everywhere is either one or zero, except at boundaries of the phases (ANSYS, 2009a). Therefore a homogeneous model or single velocity field can be used to solve these equations. The Reynolds averaging (Wilcox and Rubesin, 1980) and k-ε or shear stress transport (SST) turbulence models are used in this study. Various turbulence modelings and their application are described in ANSYS (2009a). To model the control surfaces in which flow separation is very important, SST turbulence model was used. SST blends a $k-\varepsilon$ model with a variant of $k$-$\omega$ model far from the wall, in the outer boundary layer. $k-\varepsilon$ model was used when the hull alone was modeled. The computational domain is a cuboid and the solid body is a full-scale model of the AUV. Numerical simulations are performed for both two phase flow and single phase flow. In two phase flow simulations, water and air are separated by a free surface. The numerical simulations are conducted for various vehicle submergence depths (h), with and without presence of the supporting struts. The obtained results were compared with the corresponding single phase results, in order to investigate the free surface effects on the drag and lift coefficients.

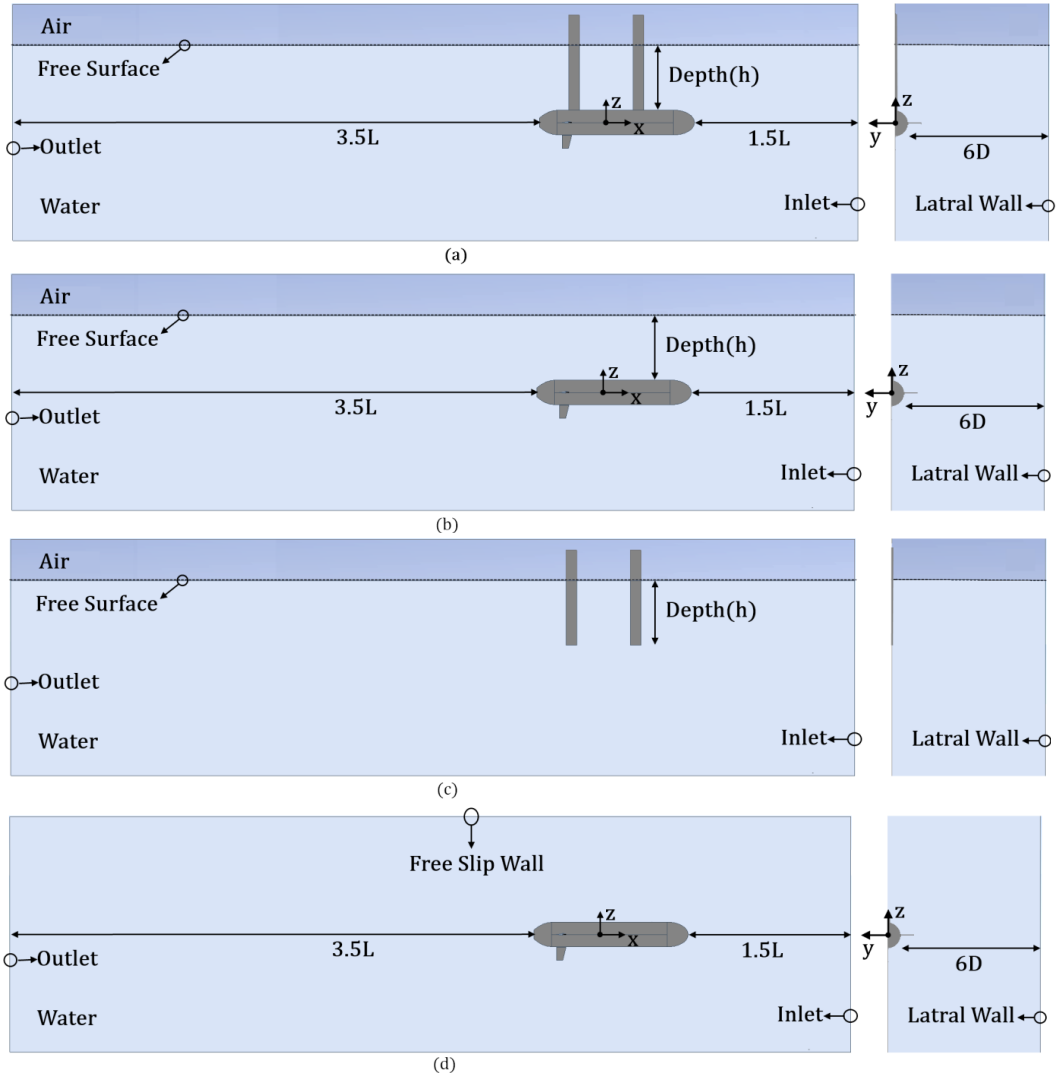


**Fig. 5. Computational domain and boundary conditions for SIM-1(a), SIM-2 (b), SIM-3 (c), SIM-4(d).**

**Table 2 Various experimental and numerical simulation conditions**

| Experimental conditions | | |
|---|---|---|
| Velocity(m/s) | Height (cm) | Non-dimensional height ($h^*$=h/D) |
| 1.5- 2.5 | 40-60 | 1.74-2.61 |
| Numerical simulation conditions | | |
| Velocity(m/s) | Height (cm) | Non-dimensional height ($h^*$=h/D) |
| 1.5- 2.5 | 20-30-40-50-60-80-90-100-120 | 0.87-1.3-1.74-2.17-2.61-3,48-3.91-4.35-5.22 |

### 3.2 Boundary Conditions

Various boundary conditions and computational domains which are used for the simulations are shown in Fig. 5. According to Table 2, various inflow velocities were specified as the inlet boundary condition. A zero relative pressure is specified as the outlet boundary condition. Free-slip boundary conditions were considered for the lateral walls, while, no slip boundary condition was used on the hull surface. For two phase flow, simulations were conducted at various AUV submergence depths, according to Table 2. Due to left and right geometrical symmetry, only half of the domain was modeled.

### 3.3 Grid Generation

The unstructured meshes, used for the simulations SIM-1 to SIM-4 are shown in Fig. 6. Similar meshes were tried to be used for the simulations in order to obtain grid independent results. A finer mesh was used near the free surface and areas with large gradients like fins and the nose of the AUV. A prism layer near the wall of quadrilateral cells was generated to resolve the high gradient boundary layer. For a specified $y^+$, the first layer thickness can be estimated (ANSYS, 2009a) as:

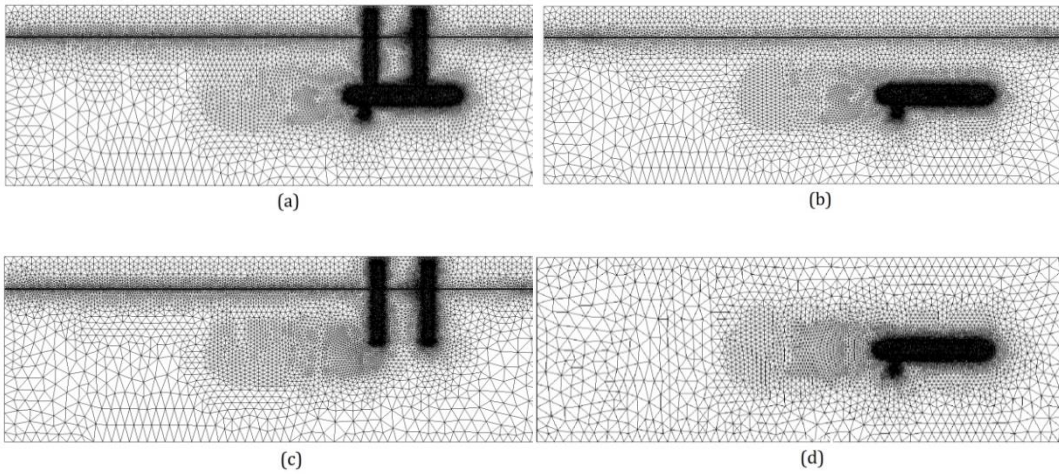


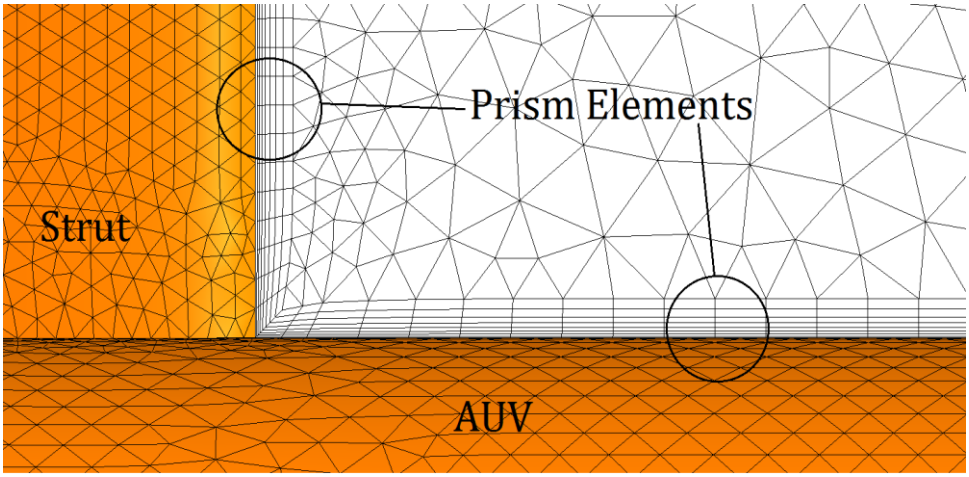


(e)

**Fig. 6. Various grids used for SIM-1(a), SIM-2 (b), SIM-3 (c), SIM-4 (d), Boundary layer (e).**

$$\Delta y = L\Delta y^{+}\sqrt{80}\,Re_L^{-\frac{13}{14}} \tag{8}$$

Boundary layer thickness $\delta_L$ can be obtained (White, 2006) using:

$$\frac{\delta_L}{L} = \frac{0.382}{Re_L^{0.2}} \tag{9}$$

For a velocity of 1.5 m/s, for example, and $y^+ = 30$, the first layer thickness and the boundary layer thickness were about 0.5105 and 29 mm, respectively. Therefore, by using an expansion factor of 1.3, the boundary layer would contain 13 layers of meshes to use for a simulation with $k-\varepsilon$ model.

### 3.4 Grid and Domain Study

In order to show that the obtained results were grid independent, for various grid sizes, the pressure coefficient $C_P$ was calculated, using Eq. (10), along lines A and B, shown in Fig. 7. Variation of $C_P$ with the non-dimensional parameter X/D for the most critical case, $v = 2.5$ m/s and h=20 cm is shown in Fig. 8. Variation of $C_P$ along these lines did not change significantly, as the number of elements increased from 2.9 million to 3.5 million elements. Therefore, use of 2.9 million elements ensured that the results were grid independent. This number of element was also numerically cost effective. A domain study was also carried out with a number of domain sizes. The domain sizes indicated in Fig. 5 were shown to be cost effective and ensured that the results were domain independent.

## 4. Numerical And Experimental Results and Analysis

Using domain and boundary conditions indicated in Fig. 5, simulations SIM-1 were performed to calculate the drag force of the AUV together with its struts at various submergence depths as well as drag forces of AUV and its struts, independently. Figure 9 shows the variation of the drag force of the AUV together with its struts as a function of submergence depth , at AUV speeds of 1.5 and 2.5 m/s. Figure 9 shows that, by increasing the submergence depth, hence the struts surface area, the total drag force of the AUV and its struts increases. Drag forces of the AUV, alone, and its struts, separately, at

$$C_P = \frac{P - P_{ref}}{0.5\rho\bar{V}^2} \tag{10}$$

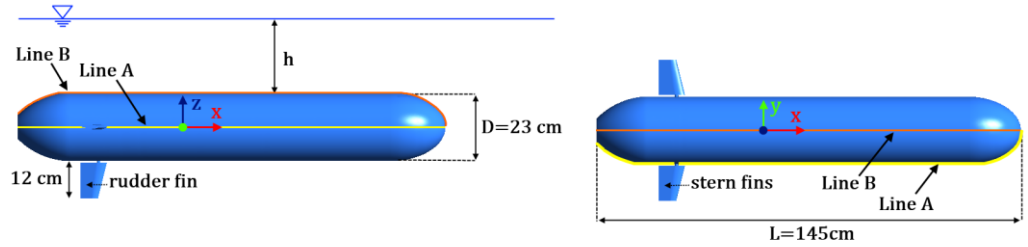


(a) Vertical Plan (z-x) (b) Horizontal Plan (x-y)

**Fig. 7. Schematic of the AUV model and the location of Line A and Line B used for Cp distribution in zox plan (a) and xoy plan (b).**

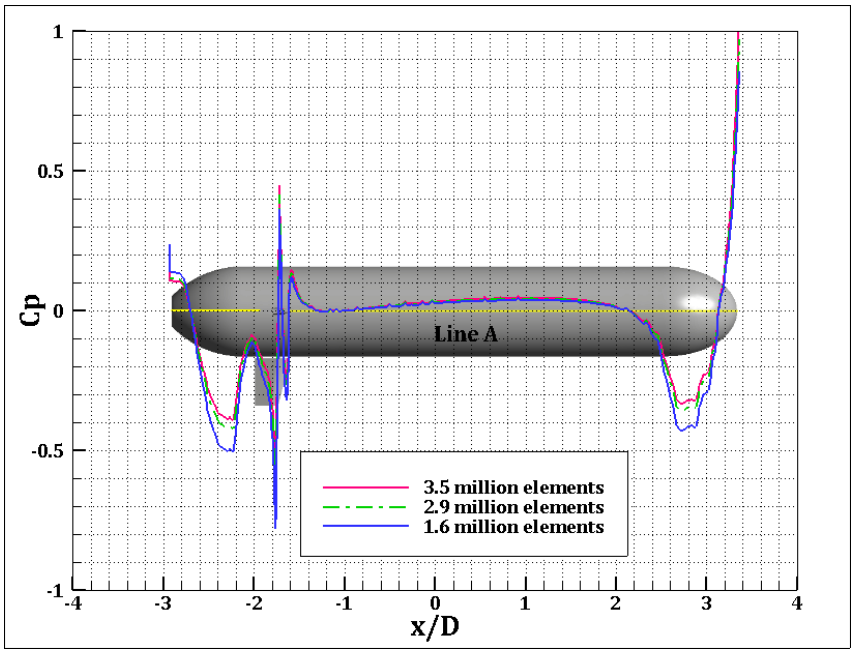


(a)

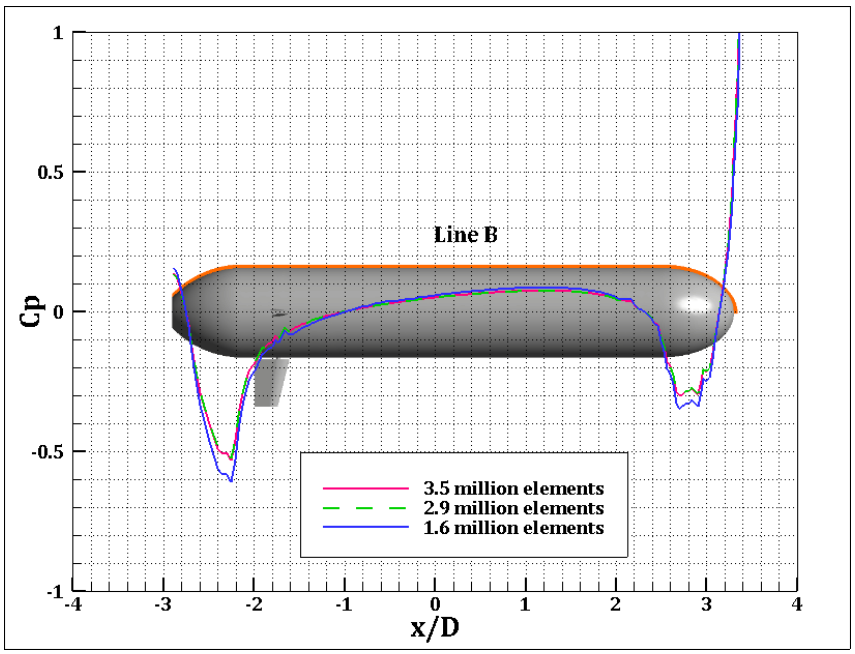


(b)

**Fig. 8. Variation of pressure coefficient with non-dimensional parameter X/D on line A (a) and line B (b), obtained for various grid sizes, $Re_l = 3.16 \times 10^6$, $h^* = 0.87$.**

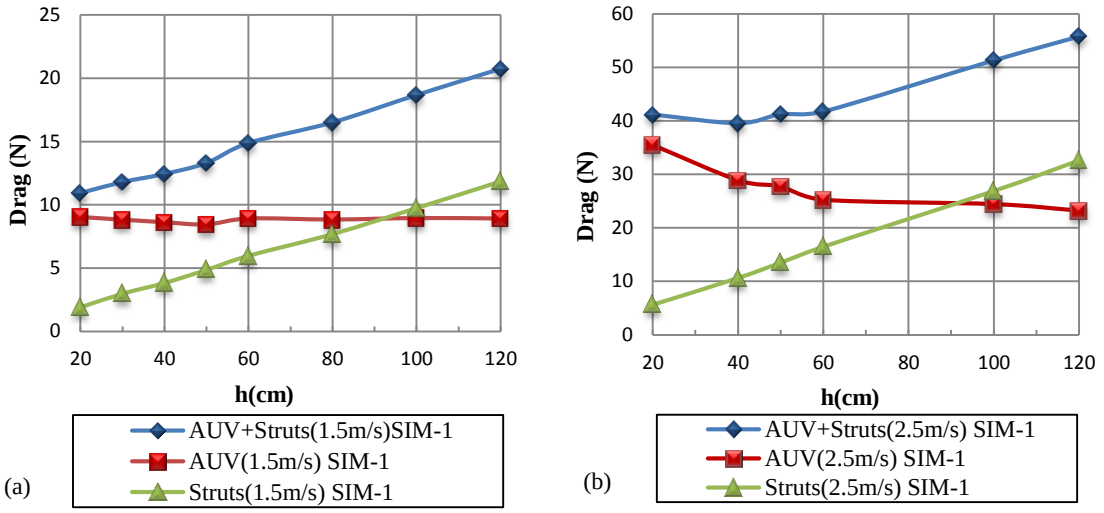


**Fig. 9. Variation of drag force with submergence depth at v=1.5m/s (a) and v=2.5m/s (b).**

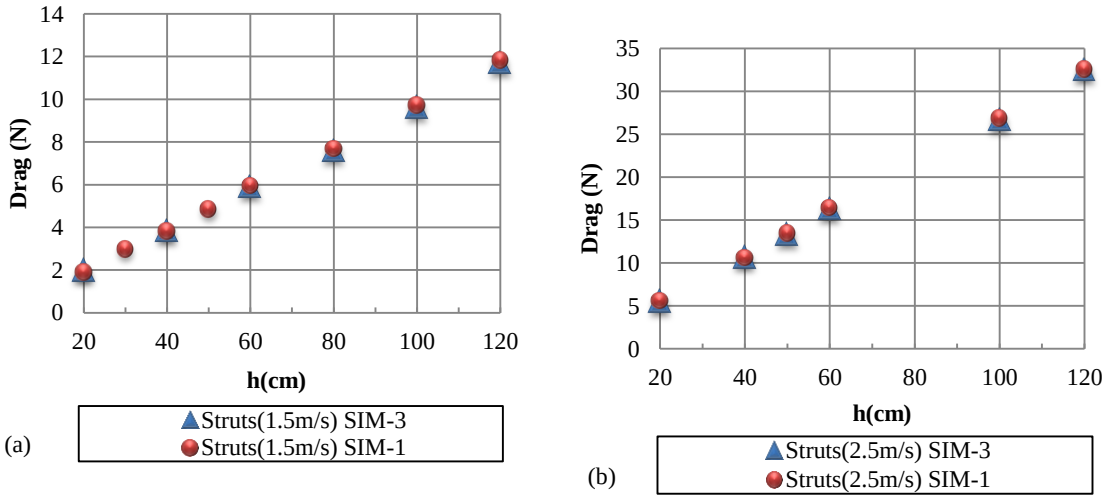


**Fig. 10. Comparing the results obtained from simulations SIM-1 and SIM-3, for the drag force of struts at v=1.5m/s (a) and v=2.5m/s (b).**

corresponding depth are also shown in this figure. As indicated in this figure, as the AUV submergence depth increases, the struts drag force increases linearly. This figure indicates that at an AUV speed of 1.5 m/s and at a submergence depth of 20 cm, the drag force ratio of the AUV to struts is about 4.7. This ratio decreases to 0.75 at a depth of 120 cm. For the AUV speed of 2.5 m/s the corresponding ratios are 6.1 and 0.71, respectively. The drag force of struts is also calculated by simulations SIM-3, in which the struts are simulated separately. The simulation results showed that drag of struts when they move separately is slightly smaller than that when they are connected to the AUV. Comparing the results obtained from simulations SIM-1 and SIM-3, for the drag force of struts, as shown in Fig. 10, indicates that, the maximum difference between two drag simulations is less than 4 percent. Non-dimensional form of this figure is shown in Fig. 11. Figure 9 shows that if a long strut is used, the drag force of the strut compared with the drag force of the AUV is large. Therefore, using Eq. (2) to calculate the AUV drag force, for a specific percent of error in calculation of the drag force of struts, results in a larger error for longer struts. We conclude from the above discussion that although using large struts (large submergence depth) decreases the influence of free surface on the drag measurement of the AUV; it introduces larger errors in Eq. (2). A numerical and experimental study conducted by Javanmard (2013) on the same AUV showed that the strut to AUV drag ratio of circular struts, at a depth of 60 cm, was more than 3, comparing with 0.67 for NACA 0012 struts. Therefore using circular struts with large drag force may result in large error in calculation of AUV drag force. To proceed our numerical investigations, it is now necessary to compare the obtained numerical results with the available experimental results. The experiments were conducted under conditions shown in Table 2. The setup of experiments were corresponded to the numerical simulations SIM-1 and SIM-3, for AUV speeds of 1.5 and 2.5 m/s and submergence depths of 40 and 80 cm. A thorough uncertainty analysis made for the experiments showed that the maximum uncertainty value of the drag coefficient was about 0.61% of the drag coefficient value. Table 3, compares the numerical and experimental results obtained for $F_{(AUV+Struts)}$

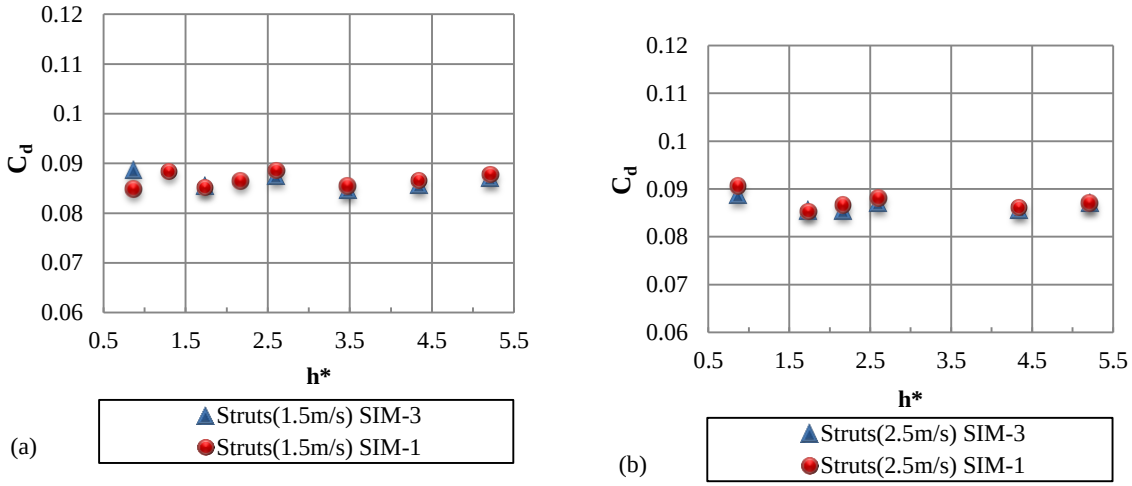


**Fig. 11. Comparing the results obtained from simulations SIM-1 and SIM-3, for the drag coefficient of struts at v=1.5m/s (a) and v=2.5m/s (b).**

**Table 3 Experimental and simulation (SIM-1 and SIM-3) results**

| Test | Velocity(m/s) | Height (cm) | Drag (N)-EXP | Drag (N)-CFD | %Diff |
|---|---|---|---|---|---|
| AUV + Struts | 1.5 | 40 | 12.9 | 12.44 | 3.57 |
| AUV + Struts | 1.5 | 60 | 14.95 | 14.88 | 0.47 |
| AUV + Struts | 2.5 | 40 | 41.01 | 39.546 | 3.57 |
| AUV + Struts | 2.5 | 60 | 43.2 | 41.725 | 3.41 |
| Struts | 1.5 | 40 | 4.027 | 3.842 | 4.59 |
| Struts | 1.5 | 60 | 5.984 | 5.89 | 1.57 |
| Struts | 2.5 | 40 | 11.1 | 10.67 | 3.87 |
| Struts | 2.5 | 60 | 17.1 | 16.29 | 4.74 |

**Table 4 Drag force obtained from Eq. (2) using experimental and numerical results**

| Velocity(m/s) | Height (cm) | Drag AUV(N)-EXP | Drag AUV (N)-CFD | %Diff |
|---|---|---|---|---|
| 1.5 | 40 | 8.873 | 8.598 | 3.1 |
| 1.5 | 60 | 8.966 | 8.99 | 0.23 |
| 2.5 | 40 | 29.91 | 28.876 | 3.46 |
| 2.5 | 60 | 26.1 | 25.435 | 2.55 |

and $F_{(Struts)}$. Using the numerical and experimental values shown in this table, the drag of AUV was calculated by Eq. (2). Table 4, compares the drag values obtained experimentally and numerically by Eq. (2). As indicated in this table, numerical results agreed well with those of experiments. The numerical results, therefore, can be used to continue our study on the effect of struts and free surface on the calculation of AUV drag force. Numerical results shown in Fig. 12 reveals that, at the AUV speed of 1.5 m/s, up to a depth of 50 cm, as the submergence depth increases, the AUV drag force decreases. However, as the submergence depth increases further, the AUV drag first increases and then, after some small oscillations, approaches to its infinite medium drag of 8.8, obtained from simulation SIM-4. The AUV drag was also calculated from SIM-2, in which the struts are removed from the AUV. The difference between the AUV drags obtained from SIM-1 and SIM-2 should, then, be only due to the presence of struts. Figure 12 compares the results obtained from these two simulations

increase of submergence depth and approaches to its infinite medium drag value. A careful observation of this figure showed that at the AUV speed of 1.5m/s, and submergence depth of 20 cm, the AUV drag obtained from simulation SIM-1 was 9.023, while, a value of 9.57 was obtained from simulation SIM-2. It means that presence of struts decreases the drag force of AUV by 6 percent. A comprehensive grid study showed that this difference was not due to the mesh structures used for two simulations. This figure shows that up to a depth of 50 cm the drag force of AUV with struts is almost 6 percent less than that without struts. This is somehow in agreement with Bertram explanation that a cylinder with a flat plate in the wake has a considerable lower resistance coefficient than a cylinder without a plate. The

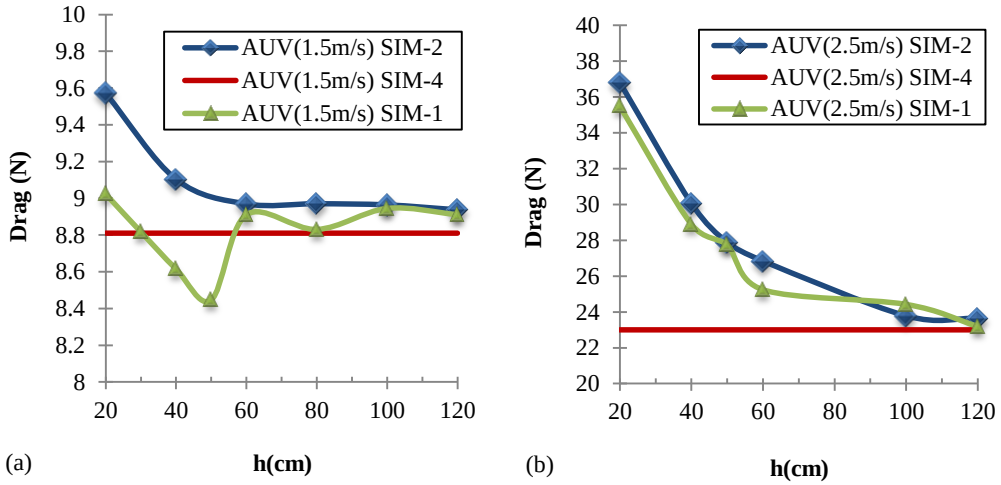


**Fig. 12. Results obtained from simulations SIM-1, SIM-2 and SIM-4 for the drag force of AUV at v=1.5m/s (a) and v=2.5m/s (b).**

reason is vortex shedding behind the cylinder with large vortices oscillating from one side to the other, see Fig. 13. These large vortex oscillations are blocked by the flat plate (Volker, 2000). One can, then, conclude that the wakes created near the free surface, as a result of AUV motion, create oscillating vortices next to the AUV body. The oscillating vortices increase the resistance force. If the AUV is connected to the struts, the oscillations can be blocked by the struts and resistance force decreases. As the submergence depth increases further, the difference between the drag force of AUV with and without struts decreases. It shows that as the free surface effect on the AUV decreases with submergence depth, the struts do not decrease the drag of AUV anymore. In this case, results obtained from SIM-1 and SIM-2, for the drag force of AUV become almost equal. In order to generalize the results obtained from the above simulations, drag coefficient is calculated as a function of relative submergence depth $(h^*=h/D)$, where, $h$ is the distance of the free surface from the AUV upper surface, and the drag value obtained for an infinite depth.

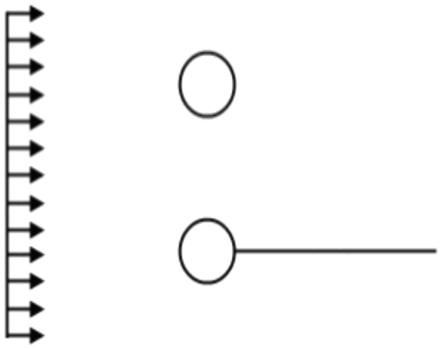

**Fig. 13. A cylinder with a flat plate in the wake has a considerable lower resistance coefficient than a cylinder without a plate.**

As shown in this figure, the drag force calculated from simulation SIM-2 continuously decreases with and $D$ is the AUV diameter. Figure 14, compares the percent of deviation of the AUV drag coefficient, obtained from simulations SIM-1 and SIM-2, from the drag coefficient obtained for an infinite medium in which there is no free surface and strut effect. This drag coefficient is denoted by $CD(\infty)$ and obtained from simulation SIM-4, as a function of relative submergence depth $h^*$, for AUV speeds of 1.5 and 2.5 m/s, corresponding to Reynolds numbers of 1.9 and 3.16 million, respectively.

As shown in this figure, simulations SIM-2 show that, at the Reynolds number of 1.9 million, the percent of deviation of AUV drag coefficient, from infinite drag coefficient, starts from 8.5 percent, at a $h^*$of 0.87, and approaches a constant value of 1.8 percent, at a $h^*$of 2.6. When struts are also simulated, in simulation SIM-1, however, the deviation starts from 2.5 percent, reaches a maximum deviation of 4 percent at $h^* = 2.17$, then, oscillates within 1 percent at higher submergence depths. To investigate the effect of AUV speed, similar simulations repeated for an AUV speed of 2.5 m/s. The results are also shown in Figs. 9(b), 10(b), 12(b) and 14(b). Almost, similar general behavior was observed in both speeds. One can conclude again, from Fig. 12 for the AUV speed of 2.5 m/s that the drag of AUV obtained from simulations including the struts (Simulation SIM-1) is smaller than that obtained from SIM-2. Although the difference between the drag of AUV obtained from simulations SIM-1 and SIM-2 is larger for speed of 2.5m/s than that for the speed of 1.5 m/s, the relative difference (difference divided by the magnitude of the AUV drag) is smaller at AUV speed of 2.5 m/s. Therefore, performing the experiments at larger speeds causes smaller relative error. Figure 14 shows that while, at a relative submergence depth of 0.87, the percent of deviation of the AUV drag coefficient from its infinite medium value was 8.5 percent for the AUV speed of 1.5 m/s, the corresponding value was 60 percent for the AUV speed of 2.5 m/s. Comparing these figures also

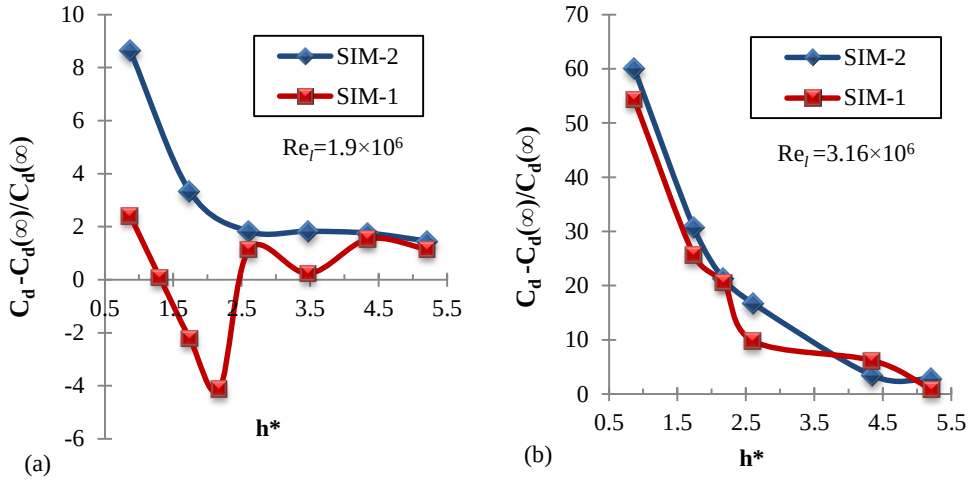


**Fig. 14. Comparing the percent of deviation of the drag coefficient as a function of relative submergence depth h*, obtained from simulations SIM-1 and SIM-2, from the drag coefficient obtained from simulation SIM-4, for an infinite medium, for Reynolds numbers of 1.9 million (a) and 3.16 million (b).**

showed that, while the AUV drag coefficient approaches its infinite medium drag value (0.189 obtained from SIM-4) at a relative submergence depth of 2.5, for an AUV speed of 1.5 m/s, the AUV drag coefficient approaches its infinite drag value (0.177 obtained from SIM-4) at a relative submergence depth of 4.34. It means that in order to eliminate the free surface effect on the drag coefficient of the AUV, longer struts should be used to conduct towing tank experiments at larger speeds. As mentioned earlier, however, longer struts introduce larger errors in Eq. (2). It is worth mentioning that using longer struts is also associated with some technical problems related to their natural frequency, which sometimes disturb the experimental results. When the length of the struts increases, the vibration frequency of the structure, including the struts and body of the AUV, gets closer to the natural frequency of the system causing high frequency oscillation in the force measured by the dynamometer. This phenomenon has been observed and documented by the authors, when two long circular struts are used instead of NACA struts.

## 5. CONCLUSION

Computational fluid dynamics was used to simulate the experimental procedure used to calculate the drag coefficient of an AUV in a towing tank. Since using struts for towing the model of the AUV in a towing tank is inevitable and there is no experimental method to investigate the effect of presence of struts on the drag coefficient of the AUV accurately, a set of numerical simulations was performed in order to investigate this effect. The effects of free surface and its interaction with both struts and AUV hull were also numerically simulated. In order to justify the obtained results, the numerical results were compared with the experimental results conducted in a towing tank. The numerical results, obtained according to the experimental procedure used to calculate the drag coefficient of the AUV, agreed well with those of experimental results. This showed that the numerical simulation can also be used to study the effect of struts and free surface on the drag coefficient of the AUV. The numerical results showed that the drag force of an AUV without struts is larger than that for an AUV with struts. The amount of difference depends on the submergence depth and speed of the AUV model in the towing tank. The numerical results showed that when the relative submergence depth increased beyond some value, this difference approached to a very small value. This was attributed to the mutual effect of free surface and struts on the drag coefficient. The numerical results also showed that when AUV speed was increased, the drag coefficient approached to its infinite drag value at larger submergence depths. Generally speaking, one can conclude that because of the presence of struts, the AUV drag obtained in a towing tank at low submergence depths is smaller than the real drag coefficient of the AUV.

## REFERENCES

*ANSYS* (2009a), Ansys-cfx Solver Modeling Guide, Release 12.1, Ansys Inc., USA.

*ANSYS* (2009b), Ansys-cfx Solver Theory Guide, Release 12.1, Ansys Inc., USA.

Barros, E. A., L. D. Dantas, A. M. Pascoal and E. de Sa (2008). Investigation of Normal Force and Moment Coefficients for an AUV at Nonlinear Angle of Attack and Sideslip Range. *Journal of Oceanic Engineering* 33(4), 583-579.

Bellevre, D., A. Diaz de Tuesta and P. Perdon (2000). Submarine Manoeuvrability Assessment Using Computational Fluid

Dynamic Tools. In *Proceeding of 23rd Symposium of Naval Hydrodynamics,* Val de Reuil, France.

Broglia, R., A. D. Mascio and G. A. Amati (2007). Parallel Unsteady RANS Code for the Numerical Simulations of Free Surface Flows. *2nd international Conference on Marine Research and Transportation,* Naples, Italy.

Gueyffier, D., J. Li, A. Nadim, R. Scardovelli and S. Zaleski (1999). Volume-of-Fluid Interface Tracking with Smoothed Surface Stress Methods for Three-Dimensional Flows. *Journal of Computational Physics* 152(2), 423-456.

Hopkin, D. and V. Hertog (1933). The Hydrodynamic Testing and Simulation of an Autonomous Underwater Vehicle. *In Proceedings of the Second Canadian Marine Dynamics Conference*, 274-281.

Jagadeesh, P. and K. Murali (2010). Rans predictions of free surface effects on axisymmetric underwater body. *Engineering Applications of Computational Fluid Mechanics* 4(2), 301-313.

Jagadeesh, P., K. Murali and V.G. Idichandy (2009). Experimental investigation of hydrodynamic force coefficients over AUV hull form. *Ocean Engineering* 36(1), 113-118.

Javanmard, E. (2013). *Determination of Hydrodynamic Coefficients of an AUV with Computational Fluid Dynamics and Experimental Fluid Dynamics Methods*. M.Sc. thesis, Isfahan University of Technology, Isfahan, Iran.

Jones, D.A., D.B. Clarke, I.B. Brayshaw, J.L. Barillon and B. Anderson (2002). *The Calculation of Hydrodynamic Coefficients for Underwater Vehicles.* DSTO Platforms Sciences Laboratory Australia.

Julca Avila, J., K. Nishimoto, J. C. Adamowski and C. Mueller Sampaio (2012). Experimental Investigation of the Hydrodynamic Coefficients of a Remotely Operated Vehicle Using a Planar Motion Mechanism. *Journal of Offshore Mechanics and Arctic Engineering* 134(2).

Krishnankutty, P., V. Anantha Subramanian, R. Francis, P. Prabhasudan Nair and K. Sudarsan (2014, June). Experimental and Numerical Studies on an Underwater Towed Body. In *Proceedings of the ASME 33rd International Conference on Ocean,* Offshore and Arctic Engineering, San Francisco, CA. 8-13.

Lafaurie, B., C. Nardone, R. Scardovelli, S. Zaleski, and G. Zanetti (1994). Modelling merging and fragmentation in multiphase flows with SURFER. *Journal of Computational Physics* 113(1), 134-147.

Malik, S. A. and P. Guang (2013). Transient Numerical Simulation for Hydrodynamic Derivatives Prediction of an Axisymmetric Submersible Vehicle. *Research Journal of Applied Science, Engineering and Technology.* 5(21), 5003-5011.

Mansoorzadeh, Sh. and E. Javanmard (2014). An investigation of free surface effects on drag and lift coefficients of an autonomous underwater vehicle (AUV) using computational and experimental fluid dynamics methods. *Journal of Fluids and Structures* 51, 161-171.

Nahon, M. (1993). Determination of undersea vehicle hydrodynamics derivatives using the USAF datcom. *In Proceedings of MTS/IEEE OCEANS*, Victoria, 283-288.

Peterson, R.S. (1980). Evaluation of semi-empirical methods for predicting linear static and rotary hydrodynamic coefficients. *Technical Report., Naval Coastal Systems Center, NCSC TM-291-80*.

Phillips, A., M. Furlong and S. R. Turnock (2007). Virtual Planar Motion Mechanism Tests of the Autonomous Underwater Vehicle Autosub. *STG-Conference/Lectureday CFD in Ship Design,* Hamburg, Germany.

Pilliod, J. E. and E. G. Puckett (2004). Second-Order Accurate Volume-of-Fluid Algorithms for Tracking Material Interfaces. *Journal of Computational Physics* 199(2), 465-502.

Rhee, K., H.K. Yoon, T.J. Sung, S.H. Kim and J.N. Kang (2000). An Experimental Study on Hydrodynamic Coefficients of Submerged Body Using Planar Motion Mechanism and Coning Motion Device. *International Workshop on Ship Manoeuvrability at the Hamburg Ship Model Basin*, Hamburg, 1-20.

Rider, W.J. and D.B. Kothe (1995). Stretching and tearing interface tracking methods. *Technical Report AIAA-95-1717, AIAA.*

Rider, W.J. and D.B. Kothe (1998). Reconstructing volume tracking. *Journal of Computational Physics* 141(2), 112-152.

Scardovelli, R. and S. Zaleski (1999). Direct numerical simulation of free-surface and interfacial flow. *Annual Review of Fluid Mechanics* 31, 567-603.

Tyagi, A. and D. Sen (2006). Calculation of transverse hydrodynamic coefficients using computational fluid dynamic approach. *Ocean Engineering* 33(5-6), 798-809.

Volker, B. (2000). *Practical Ship Hydrodynamics*. 2nd Edition.

White, F.M. (2006). *Viscous Fluid Flow*. University of Rhode Island, 3rd Edition.

Wilcox, D.C. and W.M. Rubesin (1980). Progress in turbulence modelling for complex flow fields including effects of compressibility. *NASA Technical Paper-1517*.

Wu, B. S., X. Fu and X. F. Kuang (2005). Investigation of Hydrodynamic Characteristics

of Submarine Moving Close to the Sea Bottom with CFD Methods. *Journal of Ship Mechanics* 73, 19-28.

Zhang, H., Y. R. Xu and H. P. Cai (2010). Using CFD Software to Calculate Hydrodynamic Coefficients. *Journal of Marine Science and Application* 9(2), 149-15.

Zhang, X. G. and Z. J. Zou (2013). Estimation Of The hydrodynamic Coefficients From Captive Mode Test Results By Using Support Vect*or* Machines. *Ocean Engineering* 73, 25–